Transport Powered by Bacterial Turbulence

Andreas Kaiser,[1,*] Anton Peshkov,[2,3] Andrey Sokolov,[3] Borge ten Hagen,[1] Hartmut Löwen,[1] and Igor S. Aranson[3,†]

[1]*Institut für Theoretische Physik II: Weiche Materie, Heinrich-Heine-Universität Düsseldorf, D-40225 Düsseldorf, Germany*
[2]*Laboratoire de Physique et Mécanique des Milieux Hétérogénes, Ecole Supérieure de Physique et de Chimie de la Ville de Paris, 75231 Paris Cedex 05, France*
[3]*Materials Science Division, Argonne National Laboratory, Argonne, Illinois 60439, USA*
(Received 28 January 2014; published 17 April 2014)

We demonstrate that collective turbulentlike motion in a bacterial bath can power and steer the directed transport of mesoscopic carriers through the suspension. In our experiments and simulations, a microwedgelike "bulldozer" draws energy from a bacterial bath of varied density. We obtain that an optimal transport speed is achieved in the turbulent state of the bacterial suspension. This apparent rectification of random motion of bacteria is caused by polar ordered bacteria inside the cusp region of the carrier, which is shielded from the outside turbulent fluctuations.

Suspensions of bacteria or synthetic microswimmers show fascinating collective behavior emerging from their self-propulsion [1–4], which results in many novel active states such as swarming [5–8] and active "turbulence" [9–14]. In contrast to hydrodynamic turbulence, the apparent turbulent (or swirling) state occurs at exceedingly low Reynolds numbers but at relatively large bacterial concentrations. Here we address the question of whether one can systematically extract energy out of the seemingly turbulent state established by swimming bacteria and how the bacterial turbulence may power microengines and transport mesoscopic carriers through the suspension. A related question is what processes on a scale of an individual swimmer are responsible for the energy rectification from this "active heat bath."

In our experiments we analyze the motion of a microwedgelike carrier ("bulldozer") submersed in a suspension of swimming bacteria, *Bacillus subtilis*. Experimental studies are combined with particle-resolved computer simulations. A broad span of bacterial densities is examined, ranging from the dilute regime over the turbulent one to the jammed state. Because of the activity of the suspension, the bulldozerlike particle is set into a rectified motion along its wedge cusp [15,16], in contrast to tracers with symmetric shape [17]. Its averaged propagation speed becomes maximal within the turbulentlike regime of collective swimming. Our simulations and experiment indicate that the directed motion is caused by polar ordered bacteria trapped inside the carrier in a region near the cusp which is shielded from outer turbulent fluctuations. The orientation of trapped bacteria yields a double-peaked distribution centered in the direction of the average carrier motion. Consequently, the bacterial turbulence powers efficiently the transport of carriers through the suspension.

Converting bacterial self-propulsion into mechanical energy has been considered previously for shuttles and cogwheels [18–23]. Most of the studies were restricted to low swimmer concentrations where swirling is absent. While fundamental microscopic mechanisms of energy transduction and interaction with solid walls on a scale of a single bacterium are fairly well understood, see, e.g., [24–26], the role of collective motion has not been elucidated so far. Reference [27] demonstrated that while the energy generated by individual bacteria dissipates on the microscale, the increase in swimming velocity due to collective motion is significant. Here we put forward an idea of how the collective bacterial swimming strongly amplifies the energy transduction. Complementary, in high-Reynolds-number turbulent flows, the motion of suspended inertial particles is not directed [28], lacking a conversion of turbulent fluctuations into useful mechanical work.

Experiment.— Mesoscopic wedgelike carriers were fabricated by photolithography [20,29]. To control the orientation of the carriers with an external magnetic field, we mixed a liquid photoresist SU-8 with micron-size magnetic particles before spin coating. The arm length of the wedgelike carriers is $L = 262 \ \mu$m (see Fig. 1), and the wedge angle is 90°. Experiments were conducted on a suspension of *Bacillus subtilis*, a flagellated rod-shaped swimming bacterium $\ell \sim 5 \ \mu$m long and 0.7 μm wide. The suspension of bacteria was grown for 8—12 h in Terrific Broth growth medium (Sigma Aldrich). To monitor the concentration of bacteria during the growth phase, we continuously measured the optical scattering of the medium using an infrared proximity sensor. At the end of the exponential growth phase the bacteria were washed and centrifuged to achieve the desired concentration. Then a small drop of concentrated bacterial suspension was placed between four movable fibers and stretched up to the thickness of $\sim100 \ \mu$m (see Ref. [30]). Both surfaces of the free-standing liquid film were exposed to air, significantly increasing the oxygen diffusion rate into the bulk of the film. We measured the bacteria concentration (or, equivalently, three-dimensional volume fraction) by
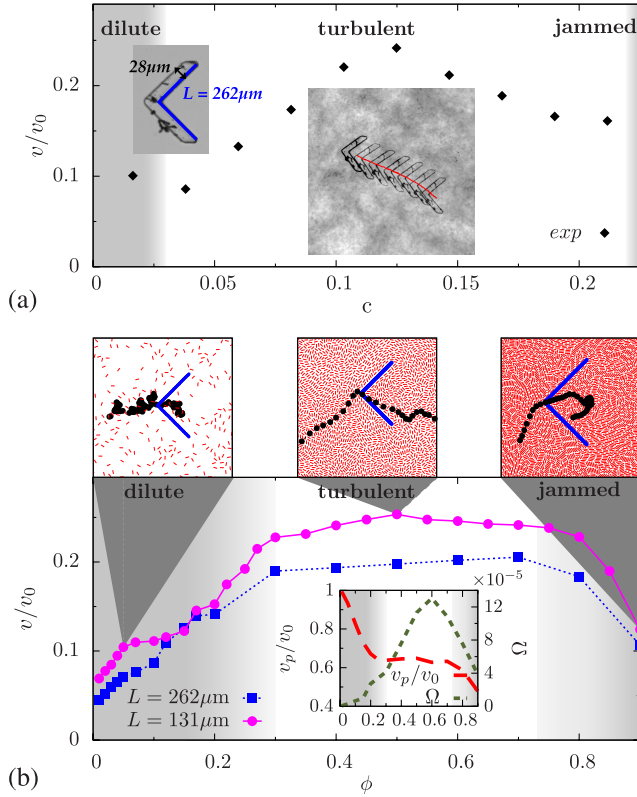
FIG. 1 (color online).   (a) Experimental carrier speed v/v_0 as a function of the bacterial three-dimensional volume fraction c. The insets show the temporal progress of the carrier positions (right) and a snapshot of the carrier (left) indicating the characteristic spatial dimensions and the schematic representation (blue line). See also movie 1 in the Supplemental Material [32]. (b) Numerically obtained transport speed for varying swimmer concentration ϕ and carriers of two different contour lengths: $L = 262$ μm (squares) corresponding to the experimental conditions and half the length $L = 131$ μm (circles). Magnitude of vorticity Ω and averaged bacterial swimming speed v_p/v_0 for various concentrations are shown in the inset. See also movies 2 and 3 in the Supplemental Material [32].

means of optical coherence tomography (see Ref. [31]) before and after the experiments in order to monitor the effect of film evaporation.

Two pairs of orthogonal Helmholtz coils were used to create a uniform magnetic field in the bulk of the liquid film. The carrier was carefully inserted in the film by a digital micropipet. In the course of our experiment, the orientation of the magnetic carrier was reversed every 20 s to prevent migration of the carrier out of the field of view. We also confirm that the average speed of the wedge does not depend on the direction of the motion. The influence of gravity was negligible in our experiment. The motion of the wedge was captured by a digital high-resolution microscope camera [Fig. 1(a) and [32]] for the duration of 2—4 min. Both displacement and orientation of the carrier were tracked by a custom-designed software based on MATLAB toolboxes.

Simulation.— We model the bacteria by rodlike objects with repulsive interactions and an effective self-propulsion using parameters matching the experimental conditions. The excluded volume interaction between the rods is described by n "Yukawa" segments positioned equidistantly with the distance $d = 0.85$ μm along a stiff axis of length ℓ; i.e., a repulsive Yukawa potential is imposed between the segments of different rods [33]. In order to properly take into account collisions between the bacteria, an important modification is introduced in the model compared to that of Ref. [11]. Experiments [26,30,34] demonstrated that two bacteria swim away from each other after the collision. This effect results in a suppression of clustering for small and moderate bacteria concentrations. However, in previous simulations [11], the bacteria had a propensity to swim parallel after the collision and to form dense clusters with a smecticlike alignment. In order to describe the experimentally observed swim-off effect and the resulting suppression of clustering, we incorporate an asymmetric effective bacterial shape by enlarging the interaction prefactor of the first segments of each rod with respect to the other segments by a factor of 3 (see [32]). The resulting total interaction potential between a swimmer pair α, β is then given by $U_{\alpha\beta} = \sum_{i=1}^{n}\sum_{j=1}^{n} U_i U_j \exp[-r_{ij}^{\alpha\beta}/\lambda]/r_{ij}^{\alpha\beta}$ with $U_1^2/U_j^2 = 3$ $(j = 2...n)$, where λ is a screening length obtained from the experimental effective rod aspect ratio $\ell/\lambda = 5$, and $r_{ij}^{\alpha\beta} = |\mathbf{r}_i^\alpha - \mathbf{r}_j^\beta|$ is the distance between segment i of rod α and segment j of rod β ($\alpha \neq \beta$). The carrier is implemented correspondingly by tiling the wedgelike contour with length $L = 262$ μm [see Fig. 1(a)] with Yukawa segments. The ratio L/ℓ is matched to the experimental situation. For comparison we also perform simulations for smaller arm lengths. The self-propulsion is taken into account via a formal effective force F_0 acting along the rod axis $\hat{\mathbf{u}} = (\cos \varphi, \sin \varphi)$. By imposing a large interaction strength $U_j^2 = 2.5 F_0 \ell$, we ensure that the bacteria and the wedge do not overlap. The model neglects long-range hydrodynamic interactions between the swimmers. These interactions do not change the overall morphology of the bacterial flow. The most noticeable effect of the hydrodynamic interactions is a 7- to 10-fold increase of the collective flow velocity compared to the speed of individual bacteria [30,35]. Certainly, this phenomenon cannot be attained by our model.

Since bacterial swimming occurs at exceedingly low Reynolds numbers, the overdamped equations of motion for the positions and orientations of the rods are

$$\mathbf{f}_{\mathcal{T}} \cdot \partial_t \mathbf{r}_\alpha(t) = -\nabla_{\mathbf{r}_\alpha} U + F_0 \hat{\mathbf{u}}_\alpha(t), \qquad (1)$$

$$\mathbf{f}_{\mathcal{R}} \cdot \partial_t \hat{\mathbf{u}}_\alpha(t) = -\nabla_{\hat{\mathbf{u}}_\alpha} U. \qquad (2)$$

Here, $U = (1/2)\sum_{\alpha,\beta(\alpha \neq \beta)} U_{\alpha\beta} + \sum_\alpha U_{\alpha<}$ is the total potential energy, where $U_{\alpha<}$ denotes the interaction energy of rod α with the carrier. (In general, a subscript $<$ refers to a quantity associated with the wedgelike carrier.) The

one-body translational and rotational friction tensors for the rods $\mathbf{f}_T$ and $\mathbf{f}_R$ can be decomposed into parallel $f_\parallel$, perpendicular $f_\perp$, and rotational f_R components which depend solely on the aspect ratio ℓ/λ and are taken from Ref. [36]. The resulting self-propulsion speed of a single rod $v_0 = F_0/f_\parallel$ is matched to the experimental value 15 μm/s [30] leading to the time unit $\tau = \ell/v_0$. Since at a relatively large bacteria concentration thermal fluctuations and tumbling are not important, we neglect all stochastic noise terms (our experimental studies in Ref. [9] showed that tumbling of *Bacillus subtilis* becomes significant only for very low oxygen concentrations). Also, hydrodynamic interaction between the bacteria and the air-water interface is neglected. According to the experiment, the motion of the carrier is mostly translational and induced by the carrier-bacteria interactions. The hydrodynamic friction tensor $\mathbf{f}_<$ of the wedge is calculated for the specific geometry with the dimensions shown in the sketch (left inset) in Fig. 1(a). For this purpose, the shape of the carrier is approximated by a large number of beads that are rigidly connected. The corresponding calculations based on the Stokes equation for the flow field around a particle at a low Reynolds number are performed with the package HYDRO++ [37,38].

The resulting equation of motion for the carrier is

$$\mathbf{f}_< \cdot \partial_t \mathbf{r}_<(t) = -\nabla_{\mathbf{r}_<} \sum_\alpha U_{\alpha<}(t). \tag{3}$$

We simulated $N \sim 10^4$ rods and a single carrier in a square simulation domain with the area $A = (3L/\sqrt{2})^2$ and periodic boundary conditions in both directions. The dimensionless packing fraction $\phi = N\lambda\ell/A$ corresponds to the bacterial volume fraction c in the experiments.

Results and discussion.— The shape reflection symmetry of the wedge around its apex will exclude any averaged directed motion perpendicular to the apex while there is no such symmetry in the apex direction. Hence, due to rectification of random fluctuations, the carrier will proceed on average along its cusp. The transport efficiency of the carrier can then be characterized by its average migration speed v in this direction. We have examined the carrier motion in a wide range of bacterial bulk concentrations including a dilute regime, where bacterial swimming is almost uncorrelated, as well as an intermediate turbulent and a final jammed regime. These regimes can be characterized by suitable order parameters. For that purpose, we define the mean magnitude of vorticity $\Omega = (1/2)\langle |[\nabla \times \mathbf{V}(\mathbf{r},t)] \cdot \hat{\mathbf{e}}_z|^2\rangle$ for a bacterial velocity field $\mathbf{V}(\mathbf{r},t)$ coarse grained over three bacterial lengths, which is a convenient indicator for bacterial turbulence [11,39]. The average swimming speed v_p of the bacteria obtained by averaging the displacements after a time $t = 10^{-3}\tau$ indicates jamming at high concentrations. Simulation results for these two order parameters are presented for a bacterial suspension in the absence of the carrier [see inset in Fig. 1(b)]. The results indicate three different states: "dilute" ($\phi \lesssim 0.25$),

"turbulent" ($0.25 \lesssim \phi \lesssim 0.75$), and "jammed" ($0.75 \lesssim \phi$). The same sequence of states is found in the experiments [40].

Figures 1(a) and 1(b) show that the transport efficiency v/v_0 of the carrier peaks in the turbulent regime where it attains a significant fraction of the net bacterial velocity v_0. Experimentally, this fraction is found to be about 0.25, which is confirmed by the simulations. Snapshots from the experiments and simulations (see insets in Fig. 1 and [32]) show a directed motion along the wedge apex though there are considerable fluctuations which we discuss later. For a very dilute regime, there are only a few bacteria pushing the carrier such that v tends to zero (note that in the experiment no motion of the carrier was observed in a very dilute regime since the resulting bacterial forces are not sufficient to overcome the friction of the carrier with the surface). We have also performed simulations for different carrier lengths and opening angles to determine the geometry leading to optimal transport. While we have chosen the optimal apex angle for our experiments, a slightly higher transport efficiency can be achieved with a smaller carrier length; see [32].

In the following we discuss the underlying reason for the optimal carrier transport in the turbulent regime. First, the bacteria inside the wedge close to the cusp are on average orientationally ordered along the wedge orientation (x direction). The orientational ordering is revealed by the intensity plots for $\langle \cos\varphi\rangle$, $\langle \sin\varphi\rangle$, which were used as appropriate orientational order parameters (see the green "hot spot" in Fig. 2). The hot spot sets the carrier into motion along the x direction. Similar to a moving bulldozer piling up sand, the carrier motion causes an accumulation
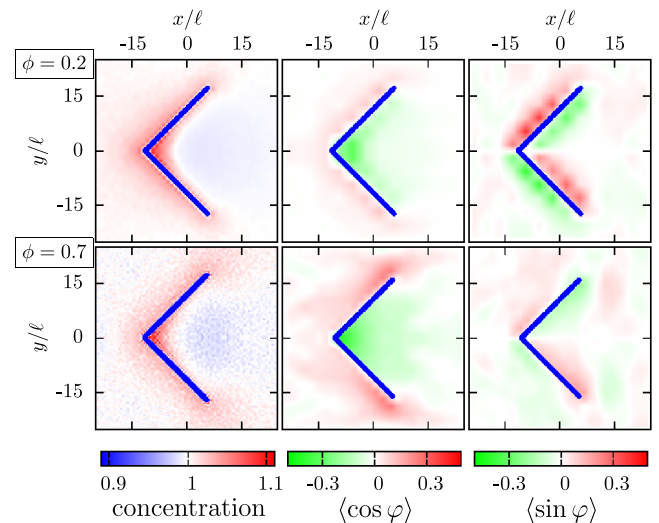

FIG. 2 (color online). Intensity plots for different bacteria concentrations, $\phi = 0.2$ (top row) and $\phi = 0.7$ (bottom row): local bacterial concentration around the carrier, normalized by the total concentration (left) as well as averaged bacteria orientations $\langle \cos\varphi\rangle$ (middle) and $\langle \sin\varphi\rangle$ (right).
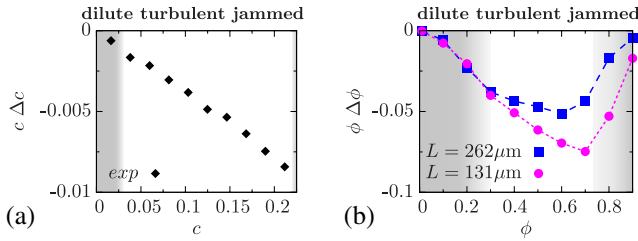
FIG. 3 (color online). Concentration difference between the wake of the carrier and its front $\Delta c = c_w - c_f$ obtained from (a) experiments and (b) simulations.

of particles in the front and a depleted wake, while not destroying the ordering of particles inside the wedge (see the intensity plot in Fig. 2 as well as Fig. 3 for experimental and simulation data for the averaged concentration difference between inside and outside bacteria). This concentration difference decreases the transport speed. But the driving effect increases with the increase in bacterial concentration. When the turbulence sets in, there is a shielding of turbulent fluctuations near the walls of the carrier (see the intensity plots of the local magnitude of vorticity in Fig. 4). The shielding is, however, more pronounced inside than outside the wedge. Intuitively this implies that the hot spot is shielded from swirls which would sweep away the driving bacteria. (Concomitantly,

the outside swirls shown in Fig. 4 are induced by the bulldozer motion but do not cause the motion.) The intuitive concept of swirl shielding is sketched in Fig. 4 where also a typical swirl size as a function of the density is shown. A typical swirl of this size can never reach the hot spot area as schematically shown by the shielded area in Fig. 4. Swimmers within this area are trapped, leading to large transport velocity correlation times for the carrier; see [32]. For simple geometric reasons, there is no such swirl shielded zone for the outside bacteria as a swirl can sweep them away. At very high concentrations ($\phi \approx 0.8$), the bacteria are jammed (see Fig. 1), which is manifested in a reduced carrier mobility. Thus, the polar order of bacteria (see intensity plots in Fig. 2) inside the wedge and its shielding from the swirls are the two basic ingredients to understand the optimal transport in the turbulent state. Optimal transport is achieved when the carrier aperture width is comparable to a typical swirl size; see [32].

We plot the full distribution of the carrier velocity direction $P(\vartheta)$ in Fig. 5(a). For small bacterial densities ϕ the distribution is random, while for intermediate concentrations this distribution exhibits a single peak centered around the x axis. For even higher concentrations it becomes double peaked, corresponding to a motion perpendicular to the single wedge walls ($\pi \pm \pi/4$). This
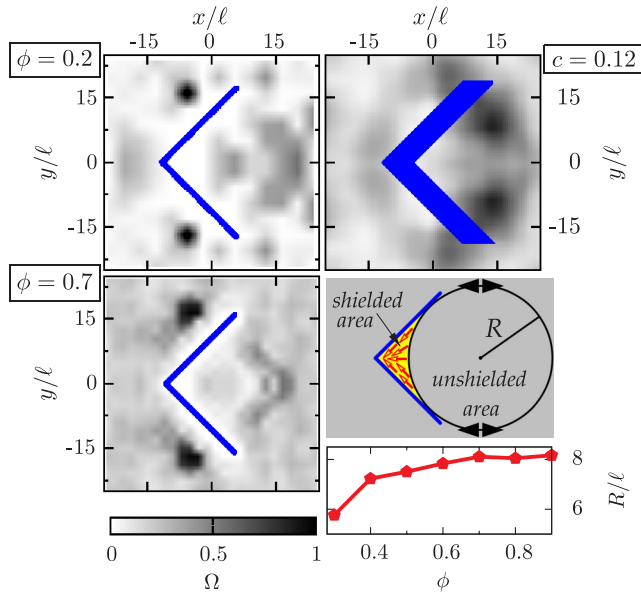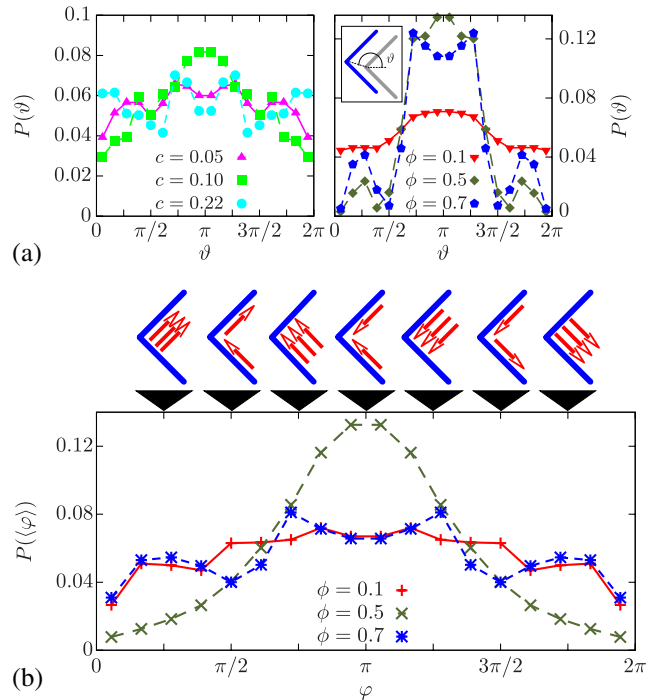

FIG. 4 (color online). Normalized local magnitude of vorticity obtained from simulations (left column) and experiment (top right). Bottom right: Illustration of swirl shielding in the carrier cusp—bacteria in the shielded area (light colored) are indicated by arrows and the unshielded area is marked by dark color. Typical swirl radius R for different bacteria concentrations is obtained as the first minimum of the equal-time spatial velocity autocorrelation function [39].

FIG. 5 (color online). (a) Probability distributions of the carrier displacement direction ϑ: Experimental results (left) measured after a time of 0.03 s and numerical results (right) after a time of $10^{-3}\tau$ for various bacterial concentrations. The definition of the displacement angle ϑ is shown in the inset. (b) Orientational ordering of the bacteria within the swirl shielded area. Characteristic configurations are illustrated by sketches.

is correlated with the orientational order distribution of the inside bacteria in the shielded area, $P(\langle\varphi\rangle)$, implying that there is a flipping in the orientation of the inside bacteria, see Fig. 5(b), for high bacterial concentrations. The kink-like change in the direction of motion perpendicular to the wedge walls is also observed experimentally [see the trajectory in Fig. 1 and peaks in Fig. 5(a)].

Conclusion.— We have shown that mechanical energy of bacterial turbulent movements can be extracted to the power directed motion of a wedgelike carrier. Both polar ordering and swirl shielding inside the wedge yield an optimal transport velocity which becomes even bidirectional at high concentrations. This effect can be exploited to power and steer carriers and motors by bacterial turbulence or the collective motion of synthetic swimmers.

[*]kaiser@thphy.uni-duesseldorf.de
[†]aronson@anl.gov

[1] M. C. Marchetti, J. F. Joanny, S. Ramaswamy, T. B. Liverpool, J. Prost, M. Rao, and R. Aditi Simha, Rev. Mod. Phys. **85**, 1143 (2013).

[2] M. E. Cates, Rep. Prog. Phys. **75**, 042601 (2012).

[3] P. Romanczuk, M. Bär, W. Ebeling, B. Linder, and L. Schimansky-Geier, Eur. Phys. J. Spec. Top. **202**, 1 (2012).

[4] I. S. Aranson, Phys. Usp. **56**, 79 (2013).

[5] V. Narayan, S. Ramaswamy, and N. Menon, Science **317**, 105 (2007).

[6] Y. Yang, V. Marceau, and G. Gompper, Phys. Rev. E **82**, 031904 (2010).

[7] X. Chen, X. Dong, A. Be'er, H. L. Swinney, and H. P. Zhang, Phys. Rev. Lett. **108**, 148101 (2012).

[8] F. Ginelli, F. Peruani, M. Bär, and H. Chaté, Phys. Rev. Lett. **104**, 184502 (2010).

[9] A. Sokolov and I. S. Aranson, Phys. Rev. Lett. **109**, 248109 (2012).

[10] D. Saintillan and M. J. Shelley, Phys. Fluids **20**, 123304 (2008).

[11] H. H. Wensink, J. Dunkel, S. Heidenreich, K. Drescher, R. E. Goldstein, H. Löwen, and J. M. Yeomans, Proc. Natl. Acad. Sci. U.S.A. **109**, 14308 (2012).

[12] K.-A. Liu and L. I, Phys. Rev. E **88**, 033004 (2013).

[13] Y. Yang, F. Qiu, and G. Gompper, Phys. Rev. E **89**, 012720 (2014).

[14] S. Zhou, A. Sokolov, O. D. Lavrentovich, and I. S. Aranson, Proc. Natl. Acad. Sci. U.S.A. **111**, 1265 (2014).

[15] P. Galajda, J. Keymer, P. Chaikin, and R. Austin, J. Bacteriol. **189**, 8704 (2007).

[16] M. B. Wan, C. J. Olson Reichhardt, Z. Nussinov, and C. Reichhardt, Phys. Rev. Lett. **101**, 018102 (2008).

[17] G. Miño, T. E. Mallouk, T. Darnige, M. Hoyos, J. Dauchet, J. Dunstan, R. Soto, Y. Wang, A. Rousselet, and E. Clement, Phys. Rev. Lett. **106**, 048102 (2011).

[18] L. Angelani, R. DiLeonardo, and G. Ruocco, Phys. Rev. Lett. **102**, 048104 (2009).

[19] L. Angelani and R. DiLeonardo, New J. Phys. **12**, 113017 (2010).

[20] A. Sokolov, M. M. Apodaca, B. A. Grzyboski, and I. S. Aranson, Proc. Natl. Acad. Sci. U.S.A. **107**, 969 (2010).

[21] D. Wong, E. E. Beattie, E. B. Steager, and V. Kumar, Appl. Phys. Lett. **103**, 153707 (2013).

[22] H. H. Wensink, V. Kantsler, R. E. Goldstein, and J. Dunkel, Phys. Rev. E **89**, 010302 (2014).

[23] R. DiLeonardo, L. Angelani, D. Dell'Arciprete, G. Ruocco, V. Iebba, S. Schippa, M. P. Conte, F. Mecarini, F. De Angelis, and E. Di Fabrizio, Proc. Natl. Acad. Sci. U.S.A. **107**, 9541 (2010).

[24] E. Lauga, W. R. DiLuzio, G. M. Whitesides, and H. A. Stone, Biophys. J. **90**, 400 (2006).

[25] G. Li and J. X. Tang, Phys. Rev. Lett. **103**, 078101 (2009).

[26] K. Drescher, J. Dunkel, L. H. Cisneros, S. Ganguly, and R. E. Goldstein, Proc. Natl. Acad. Sci. U.S.A. **108**, 10940 (2011).

[27] T. Ishikawa, N. Yoshida, H. Ueno, M. Wiedeman, Y. Imai, and T. Yamaguchi, Phys. Rev. Lett. **107**, 028102 (2011).

[28] E. Calzavarini, M. Cencini, D. Lohse, and F. Toschi, Phys. Rev. Lett. **101**, 084504 (2008).

[29] J. Gachelin, G. Miño, H. Berthet, A. Lindner, A. Rousselet, and É. Clément, Phys. Rev. Lett. **110**, 268103 (2013).

[30] A. Sokolov, I. S. Aranson, J. O. Kessler, and R. E. Goldstein, Phys. Rev. Lett. **98**, 158102 (2007).

[31] A. Sokolov, R. E. Goldstein, F. I. Feldchtein, and I. S. Aranson, Phys. Rev. E **80**, 031903 (2009).

[32] See Supplemental Material at http://link.aps.org/supplemental/10.1103/PhysRevLett.112.158101 for movies and additional data.

[33] T. Kirchhoff, H. Löwen, and R. Klein, Phys. Rev. E **53**, 5011 (1996).

[34] I. S. Aranson, A. Sokolov, J. O. Kessler, and R. E. Goldstein, Phys. Rev. E **75**, 040901 (2007).

[35] C. Dombrowski, L. Cisneros, S. Chatkaew, R. E. Goldstein, and J. O. Kessler, Phys. Rev. Lett. **93**, 098103 (2004).

[36] M. M. Tirado, C. L. Martinez, and J. G. de la Torre, J. Chem. Phys. **81**, 2047 (1984).

[37] J. Garcia de la Torre, S. Navarro, M. C. Lopez Martinez, F. G. Diaz, and J. J. Lopez Cascales, Biophys. J. **67**, 530 (1994).

[38] B. Carrasco and J. Garcia de la Torre, J. Chem. Phys. **111**, 4817 (1999).

[39] H. H. Wensink and H. Löwen, J. Phys. Condens. Matter **24**, 464130 (2012).

[40] A. Sokolov and I. S. Aranson, Phys. Rev. Lett. **103**, 148101 (2009).